Electronic Supplementary Information

Distinct reconstruction of aluminum-doped oxide-derived copper enhances selectivity of C_{2+} products in CO_2 electroreduction

Junghwan Jang,[‡a,b] Kangjae Lee,[‡a,b] Heejong Shin,[a,b] Hyeon Seok Lee,[a,b] Byoung-Hoon Lee,[a,b] Juwon Jeong,[a,b] Jungho Kim,[c] Wonchan Hwang,[a,b] SungBin Park,[a,b] Megalamane S. Bootharaju,[a,b] Seoin Back,[c] Jaehyuk Shim,[a,b] Jeong Hyun Kim,[a] Taeghwan Hyeon,*[a,b] and Yung-Eun Sung*[a,b]

[a]Center for Nanoparticle Research, Institute for Basic Science (IBS), Seoul 08826, Republic of Korea.

[b]School of Chemical and Biological Engineering, Seoul National University, Seoul 08826, Republic of Korea.

[c]Department of Chemical and Biomolecular Engineering, Institute of Emergent Materials, Sogang University, Seoul, 04107, Republic of Korea

‡ These authors contributed equally to this work.

*Corresponding authors. E-mail: thyeon@snu.ac.kr (T. Hyeon), ysung@snu.ac.kr (Y. -E. Sung)

Experimentals

Materials

Copper(II) nitrate trihydrate ($Cu(NO_3)_2 \cdot 3H_2O$, 99-104%), Trimesic acid ($C_6H_3(CO_2H)_3$, 95%), Aluminum acetylacetonate ($Al(acac)_3$, 99%), potassium bicarbonate ($KHCO_3$, ≥ 99.5%), potassium hydroxide (KOH, ≥ 85%), potassium sulfate (K_2SO_4, ≥ 99.0%), 5 wt% Nafion solution, benzotriazole ($C_6H_5N_3$, 99%), sodium perchlorate ($NaClO_4$, ≥ 98%), perchloric acid ($HClO_4$, 70%), and lead(II) perchlorate hydrate ($PbClO_4 \cdot xH_2O$, ≥ 99.995%) were purchased from Sigma-Aldrich. Methanol and isopropanol (≥ 99.9%) were provided by Samchun chemicals (Republic of Korea).

Synthesis of HKUST-1 and HKUST-1 ($Al_{0.35}$)

For the synthesis of HKUST-1, it was slightly changed from previous methods. [1] 875 mg of trimesic acid was dissolved in 40 ml methanol to make solution A. 2416 mg of $Cu(NO_3)_2 \cdot 3H_2O$ (10 mmol) was dissolved in 40 ml methanol to make solution B. Then, the two solutions were mixed, stirred at 700 rpm for 1 h, and kept overnight at room temperature. The as-obtained precipitate was centrifuged with methanol 3 times to remove excess copper ions and trimesic acid. Finally, the product was dried in a vacuum oven overnight. HKUST-1 ($Al_{0.35}$) was synthesized in the same procedure except that 113 mg of $Al(acac)_3$ (0.35 mmol) was additionally dissolved in solution B.

Synthesis of CuO and CuO_Al

To prepare CuO, HKUST-1 was heated at 400 ℃ for 1 h in a muffle furnace at a

5 ℃/min ramp rate under the air. Preparation of CuO_Al was following the same procedure using HKUST-1 ($Al_{0.35}$). After annealing, both catalysts are ground in a mortar.

Materials characterizations

Transmission electron microscopy (TEM) imaging, high-resolution transmission electron microscopy (HRTEM) imaging, and scanning transmission electron microscopy(STEM) imaging with energy-dispersive X-ray spectroscopy (EDS) mapping were carried out on a transmission electron microscope (JEM-2100F, JEOL) equipped with a single drift detector (X-MAXN, Oxford Instruments) at 200 kV. Scanning electron microscopy (SEM) imaging was performed on a scanning electron microscope (SUPRA 55-VP, Carl Zeiss) at 2 kV. Thermogravimetric analysis (TGA) was conducted by a thermogravimetric analyzer (SDT-Q600, TA instruments) in the air at a ramp rate of 10 ℃ min^{-1} and flow rate of 10 ml min^{-1}. X-ray diffraction (XRD) patterns of samples on carbon paper were obtained on an X-ray diffractometer (Smartlab XRD, Rigaku) with Cu K_α radiation in the range of 20-80° (2θ) with a step size of 0.01°. X-ray photoelectron spectroscopy (XPS) spectra were acquired on an X-ray photoelectron spectrometer (K-alpha, Thermo Fisher Scientific) with Al K_α radiation and the C_{1s} peak was calibrated at 284.6 eV. X-ray absorption fine structure (XAFS) measurement at Cu K-edge was conducted at the 8C beamline of Pohang Accelerator Laboratory (PAL, Republic of Korea). Cu foil was used to calibrate Cu K-edge energy (E_0=8978.9 eV) and fluorescence yield detection was used to gain Cu K-edge spectra. IFEFFIT package including ATHENA and Artemis was used to process XAFS spectra and fitting of EXAFS spectra Concentrations of Cu and Al in the sample were measured by an inductively coupled plasma atomic emission spectrometer (OPTIMA 8300, Perkin-Elmer) installed at the National Center for Inter-university Research Facilities (NCIRF) of Seoul National University.

Electrodes preparation

To prepare electrodes, catalyst ink was spray-coated onto the gas-diffusion layer (GDL). 10 mg of the catalyst was mixed with 20 µl of 5 wt% Nafion solution and 3 ml of isopropanol solvent. The catalyst ink was sonicated for 30 min to form a homogeneous suspension and spray-coated onto a gas diffusion layer (JNT30-A6H, JNTG Co., Republic of Korea) using an airbrush (Hi-Line HP-CH, ANEST IWATA). The gas diffusion electrode (GDE) was dried in an oven at 60 °C overnight. The GDE before and after catalyst loading was weighed to determine the loading amount and it was approximately 0.5 mg cm^{-2}.

Electrochemical measurements

All of the electrochemical measurements were performed in a custom-made flow cell with a three-electrode system connected to an electrochemical workstation (PGSTAT302N, Metrohm Autolab). The GDE, a Ni foam (Alantum Co., Republic of Korea) electrode, and Ag/AgCl electrode (RE-1CP, ALS Co., Japan) filled with saturated KCl solution were used as working, counter, and reference electrodes, respectively. 1M $KHCO_3$ was used as the catholyte and anolyte, which were separated by an anion exchange membrane (Sustainion® X37-50 Grade RT membrane, Dioxide Materials). Both electrolytes were circulated through each compartment of the flow cell at 20 sccm by using a dual-channel peristaltic pump (Masterflex L/S series, Cole-Parmer). High-purity CO_2 (5N, KS TECH Co., Republic of Korea) was purged at 30 sccm to the cathode chamber and passed through the catalyst layer from the backside of GDE. Before all of the electrochemical measurements, samples were electrochemically reduced to OD-Cu by applying 1 mA for 15 min under Argon (Ar) conditions.

eCO_2RR performance was measured under galvanostatic conditions, applying reductive currents from 100 mA to 700 mA with a 100-mA step. The linear sweep voltammetry

(LSV) was conducted at a scan rate of 10 mV s^{-1} in the potential range from -0.1 V to -0.9 V (vs. RHE). The stability test was performed at 300 mA with the same configurations but a small amount of 1M $KHCO_3$ electrolyte was continuously added to the catholyte for suppressing pH change in the catholyte. The electrochemical impedance spectroscopy (EIS) was carried out on electrochemically reduced OD-Cu samples at 10 mA in the frequency range from 10^5 to 0.1 Hz. Nyquist plots were obtained from EIS measurement and were fitted by Zview software (Scribner Associates). Ohmic drop by solution resistance was corrected for all of the electrochemical measurements. The Nova software and FRA2 module (Metrohm Autolab) were used to correct 85% of ohmic drop and uncompensated ohmic drop was corrected manually. All potentials were converted to the reversible hydrogen electrode (RHE) scale by equation (1). [2]

$$E\ (\text{vs. RHE}) = E\ (\text{vs. Ag/AgCl}) + 0.197\ \text{V} + 0.05916 \times \text{pH} \quad (1)$$

Product analysis

The gas products and liquid products were quantified by gas chromatography (GC) and ^{1}H nuclear magnetic resonance (^{1}H NMR). The cathode compartment of the flow cell is connected to GC (7890B, Agilent), so effluent streams from eCO_2RR were routed into the gas sampling loop of the GC. Gas products in effluent streams were analyzed by a flame ionization detector and thermal conductivity detector. Catholyte after eCO_2RR was mixed with D_2O and sodium 2,2-Dimethyl-2-silapentane-5-sulfonate (DSS) as an internal standard. Then the sample is analyzed by ^{1}H NMR spectrometer (AVANCE III 600, Bruker) with water suppression. The amounts of the products resulting from GC and ^{1}H NMR were used to calculate the Faradaic efficiency (FE) of products with the following equation: [3]

$$\text{FE}\ (\%) = \frac{\text{amount of the product} \times n \times F}{C} \times 100 \quad (2)$$

where n is the number of electrons participating in the Faradaic reaction to produce one molecule, F is the Faraday constant (96485 C mol^{-1}), and C is the quantity of charge participating in the Faradaic reaction.

For gas and liquid products, equation (2) can be expressed as following equations: [4]

$$\text{FE}_{\text{gas}}\ (\%) = x_i \times v \times \frac{\text{P}_0}{RT} \times \frac{n_i \times \text{F}}{I_{\text{total}}} \times 100 \quad (3)$$

$$\text{FE}_{\text{liquid}}\ (\%) = \frac{N_i \times n_i \times \text{F}}{I_{\text{total}} \times \Delta t} \times 100 \quad (4)$$

where x_i is the volume fraction of gas product i, v is the gas flow rate entering the GC sampling loop, P_0 is the ambient pressure, R is the gas constant, T is the temperature, n_i is the number of electrons participating in the Faradaic reaction to produce one molecule of the product i, I_{total} is the total current of Faradaic reaction, N_i is the amount of product i produced per reaction time Δt. The products contain H_2, CO, HCOOH, CH_4, C_2H_4, C_2H_5OH, CH_3COOH, and C_3H_7OH.

Cu passivation

Cu passivation with benzotriazole (BTA) was carried out by replacing the catholyte with BTA solution right after eCO_2RR. The BTA solution is made by saturating BTA in 1M $KHCO_3$ solution and purging Ar gas for sufficient time to remove oxygen in the solution.

ECSA measurement

Lead underpotential deposition (Pb UPD) and double-layer capacitance method were performed to measure the electrochemically active surface area (ECSA).

For Pb UPD, a 100 mM $NaClO_4$ electrolyte with 10 mM $HClO_4$ and 3 mM $Pb(ClO_4)_2$ was made and used as the electrolyte. [5] The electrolyte was purged with Ar and the samples were electrochemically reduced before Pb UPD. The Hg/Hg_2SO_4 electrode (5100A, Koslow Scientific Co.) with saturated potassium sulfate was used as the reference electrode to exclude the influence of chloride ion on Pb UPD. [6] Cyclic voltammetry was conducted from -0.84 to -0.49 V (vs. Hg/Hg_2SO_4) at the scan rate of 10 mV s^{-1} and it was repeated until the two consecutive scan cycles coincided. The anodic peak of the last scan cycle (Pb stripping peak) was integrated and divided by the area of Cu foil and the loading amount to determine ECSA (m^2 g_{Cu}^{-1}).

For double-layer capacitance measurement, Ar-purged 1 M $KHCO_3$ electrolyte was used as the electrolyte and samples were electrochemically reduced before measurement. The same configurations were used and cyclic voltammetry (CV) was conducted from 0.225 to 0.325 V (vs. RHE) at the scan rates of 10, 15, 20, 25, 30, 35, and 40 mV s^{-1}. It was also repeated until the two consecutive scan cycles coincided. The capacitance was calculated by following equation: [7]

$$\frac{I_a - I_c}{2} = Cv \tag{5}$$

where I_a is the anodic current at 0.325 V (vs. RHE), I_c is the cathodic current at 0.225 V (vs. RHE), C is the capacitance, and v is the scan rate. The capacitance can be derived by plotting the left side of equation (5) against the scan rate. The ECSA is proportional to the capacitance.

Contact angle measurement

The contact angle was measured by droplet on the sample. The contact angle of the droplet was measured by an optical contact angle measurement system (Phoenix-MT series, SEO Co., Republic of Korea) at room temperature. The spray-coated electrodes were used as samples and the volume of water drop was 4 μl. The contact angle was averaged by measuring five different positions of the same sample. The electrodes after eCO_2RR were rinsed with deionized water and dried in an oven overnight.

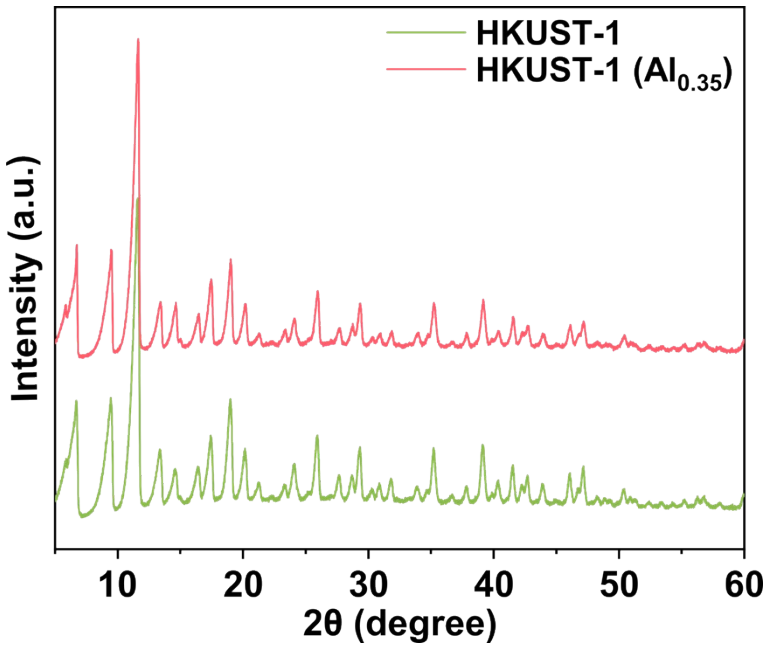

Figure S1. XRD patterns of HKUST-1 and HKUST-1 with Al precursor before calcination.

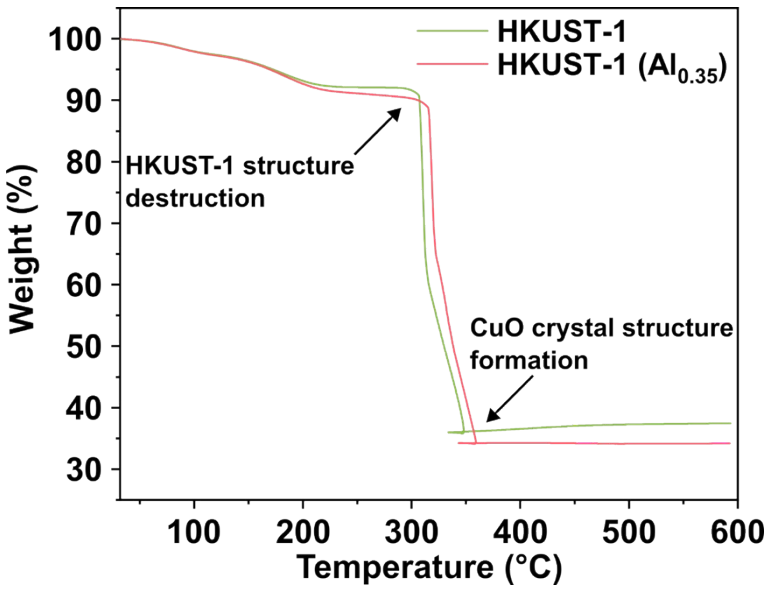

Figure S2. TGA curves of HKUST-1 and HKUST-1 with Al precursor at a ramp rate of 10 °C min^{-1}.

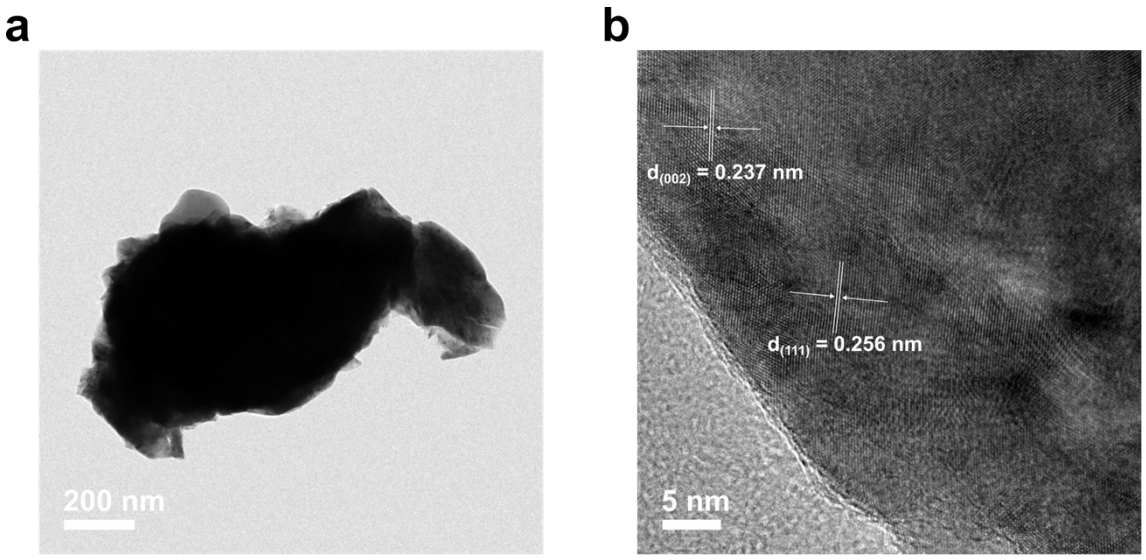

Figure S3. (a) TEM and (b) HRTEM image of CuO after synthesis.

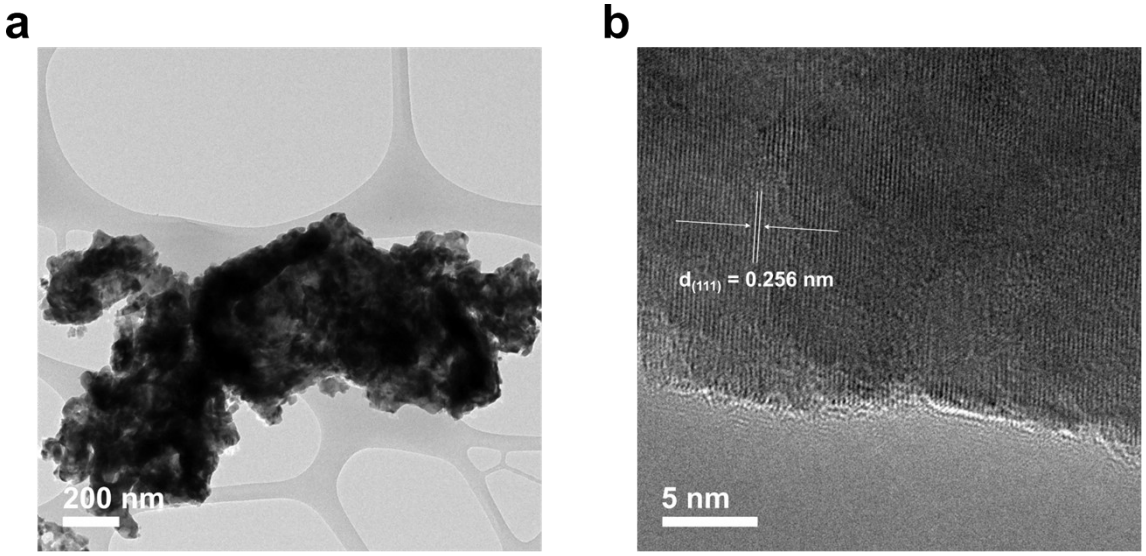

Figure S4. (a) TEM and (b) HRTEM image of CuO_Al after synthesis.

a

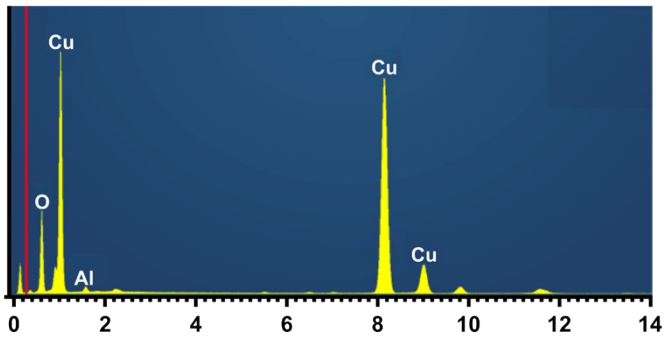

b

Element	Wt%
Cu	80.2
O	19.0
Al	0.8

Figure S5. (a) EDS spectrum of CuO_Al from STEM-EDS and (b) its calculated chemical composition.

Element	Concentration(ppm)	Wt%	At%
Cu	839890.21	99.19	98.10
Al	6894.51	0.81	1.90
Cu/Al	-	121.82	51.72

Table S1. Concentration and chemical composition of Cu and Al in CuO_Al analyzed by ICP-AES.

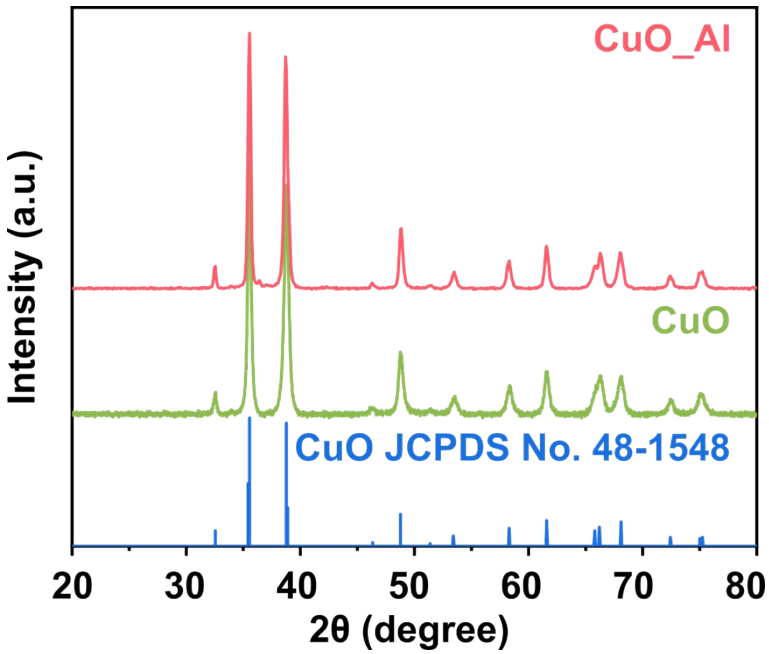

Figure S6. XRD patterns of CuO and CuO_Al after synthesis.

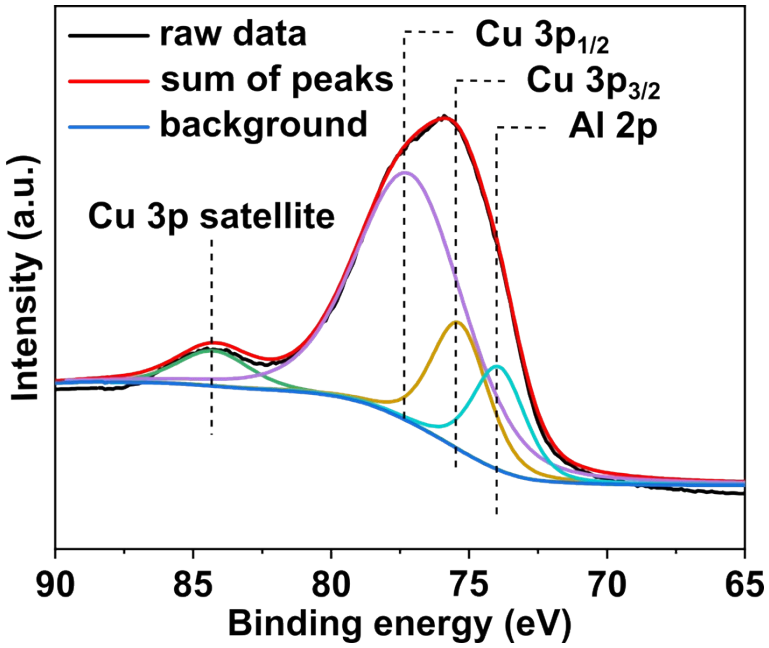

Figure S7. Deconvoluted XPS spectra of Al 2p for CuO_Al. Deconvolution was carried out with the XPSpeak41 program, fixing %GL (gaussian and Lorentzian percentage) and peak position.

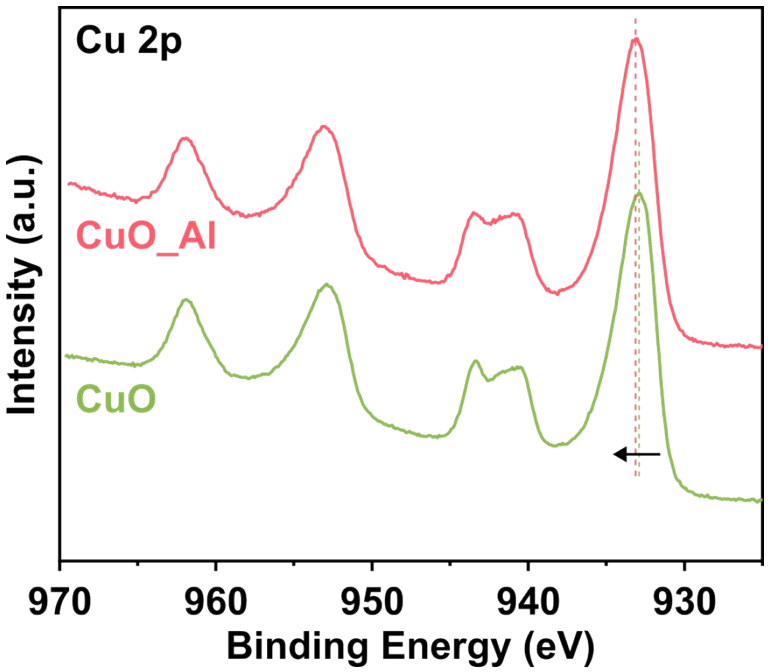

Figure S8. XPS spectra of Cu 2p for both catalysts. Dashed lines indicate Cu $2p_{3/2}$ peak positions.

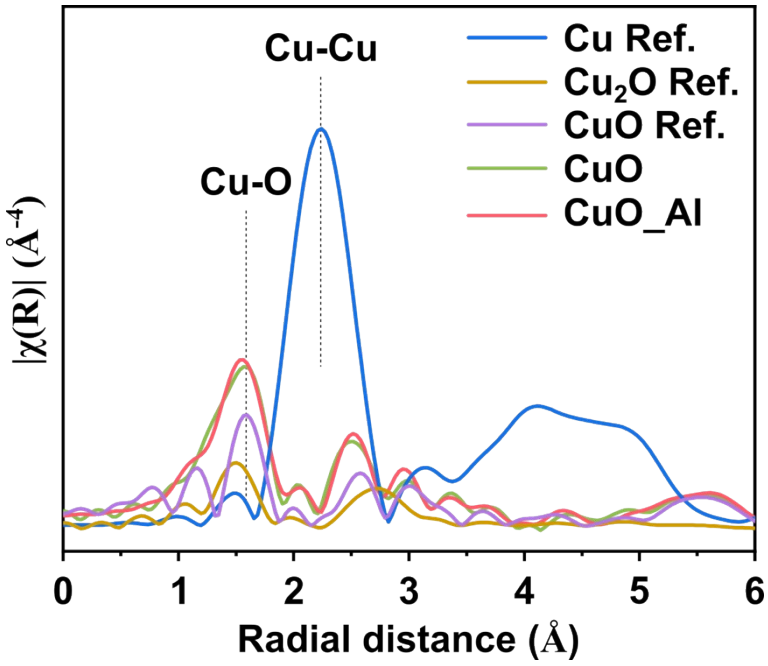

Figure S9. Cu K-edge FT-EXAFS spectra of both catalysts and reference samples. Dashed lines indicate the positions of Cu-O and Cu-Cu peaks.

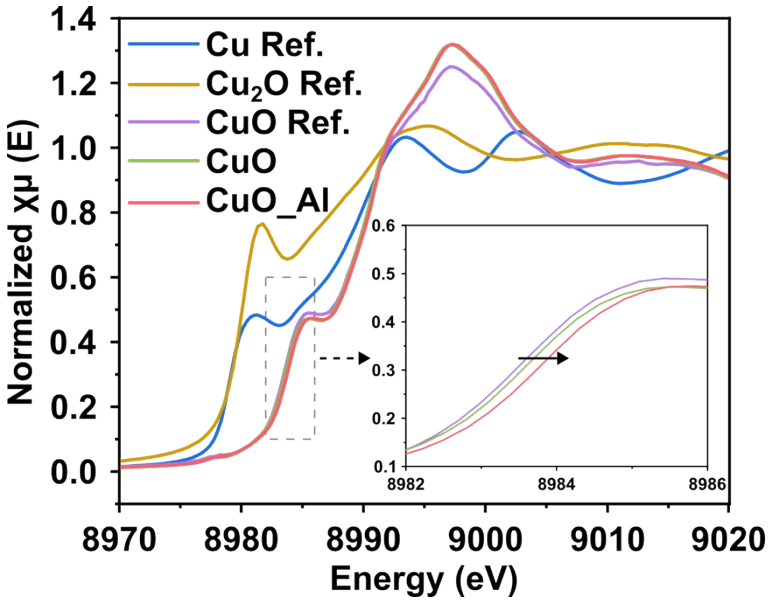

Figure S10. Cu K-edge XANES spectra of both catalysts and reference Cu foil. The insets magnify the absorption edge of both catalysts.

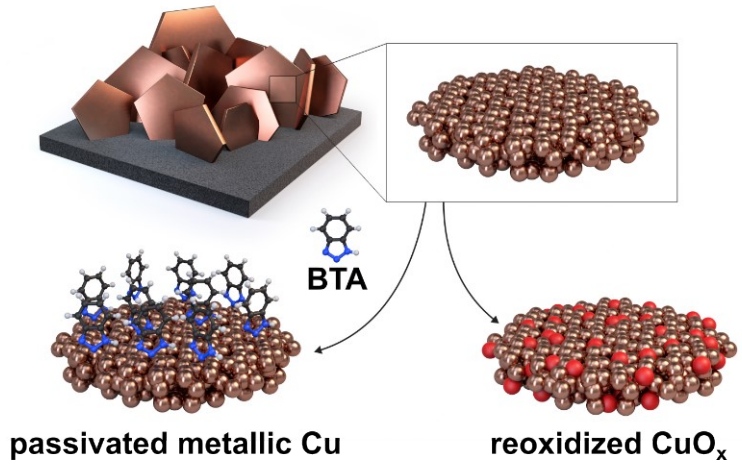

Figure S11. Schematic illustration of Cu passivation by BTA.

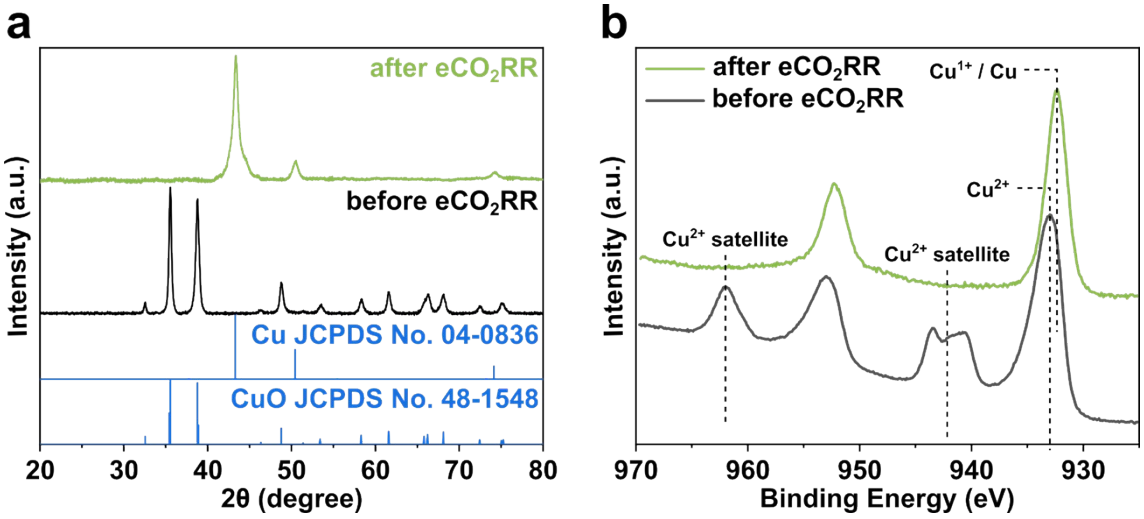

Figure S12. (a) XRD patterns and Cu 2p XPS spectra of CuO before and after eCO_2RR.

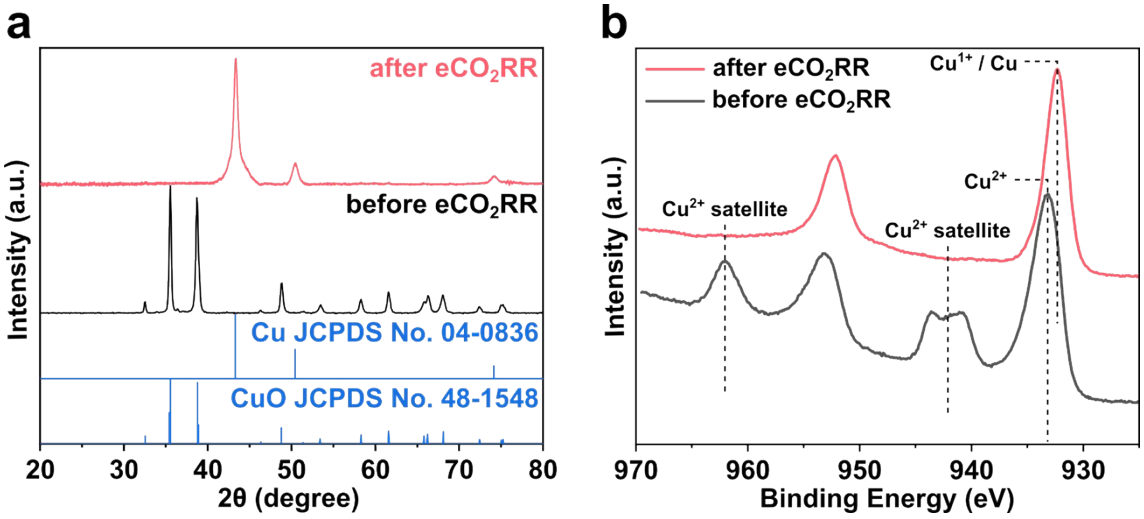

Figure S13. (a) XRD patterns and Cu 2p XPS spectra of CuO_Al before and after eCO_2RR.

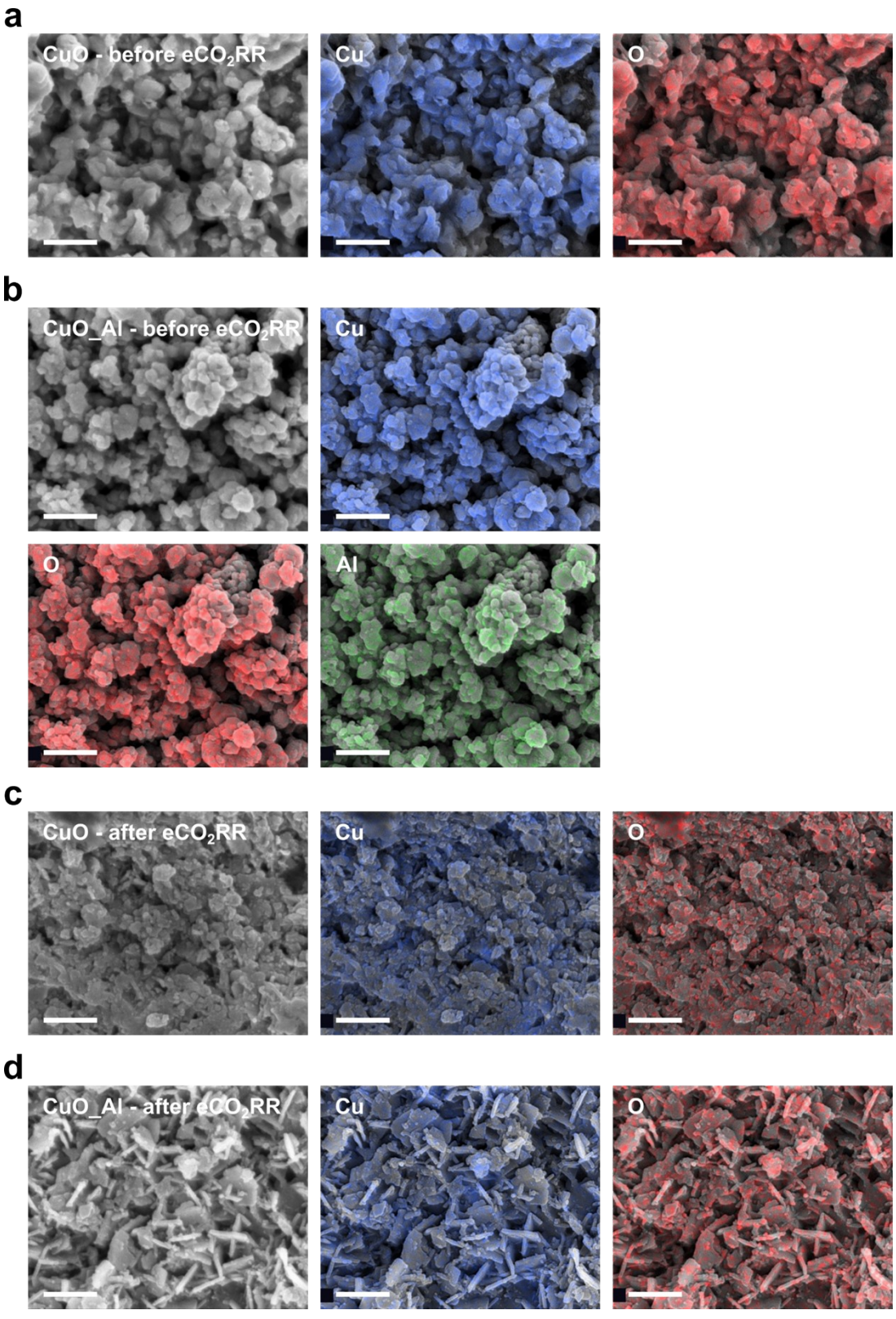

Figure S14. SEM images and corresponding EDS mapping images of (a) CuO and (b) CuO_Al before eCO_2RR and (c) CuO and (d) CuO_Al after eCO_2RR (scale bars: 1 μm).

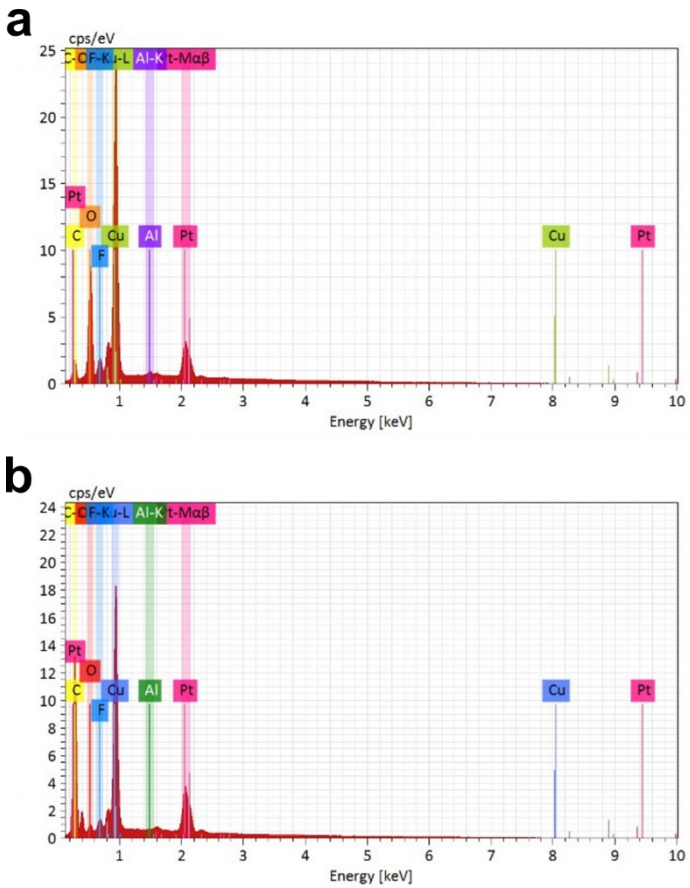

c

Element	Cu (wt%)	O (wt%)	Al (wt%)	C (wt%)
CuO before eCO_2RR	78.24	15.87	0.00	5.87
CuO_Al before eCO_2RR	77.56	16.28	0.53	5.62
CuO after eCO_2RR	55.92	1.27	0.00	42.80
CuO_Al 0.5 min eCO_2RR	50.14	1.39	0.07	48.39
CuO_Al after eCO_2RR	59.18	0.97	0.00	39.85

Figure S15. EDS spectra of CuO_Al (a) before eCO_2RR and (b) after eCO_2RR from SEM-EDS. (c) Calculated chemical composition of CuO and CuO_Al before and after eCO_2RR.

EDS spectra of all samples contain Pt and F. Pt signals come from Pt coating before SEM for high resolution in SEM imaging by high conductivity. F signals come from the PTFE-coated carbon substrate (JNT30-A6H, JNTG Co., Republic of Korea) for high hydrophobicity.

Increased carbon composition after eCO_2RR comes from BTA adsorption (Cu passivation), and nanoflakes do not consist of carbon due to the high composition of carbon in CuO after eCO_2RR. The absence of the K signal eliminates the possibility of K_2CO_3 salt. Therefore, there are no other impurities to explain the formation of nanoflakes.

a

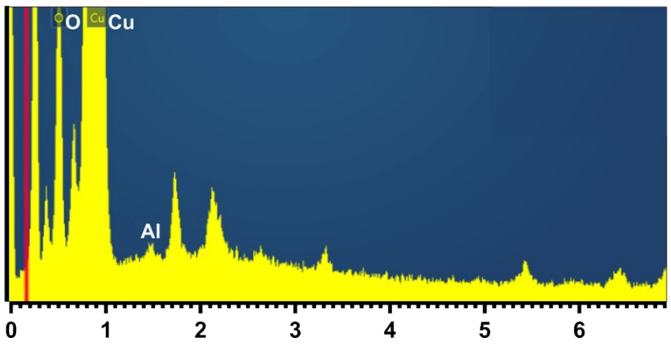

b

Element	Wt%
Cu	94.9
O	5.0
Al	0.1

Figure S16. (a) EDS spectrum of CuO_Al after eCO_2RR from STEM-EDS and (b) its calculated chemical composition.

Element	0 min (wt%)	0.5 min (wt%)	5 min (wt%)	60 min (wt%)
Cu	99.13	99.74	99.79	99.93
Al	0.87	0.26	0.21	0.07

Table S2. Chemical compositions of Cu and Al in CuO_Al electrodes during eCO_2RR for 0, 0.5, 5, and 60 min at 500 mA cm^{-2} by ICP-AES.

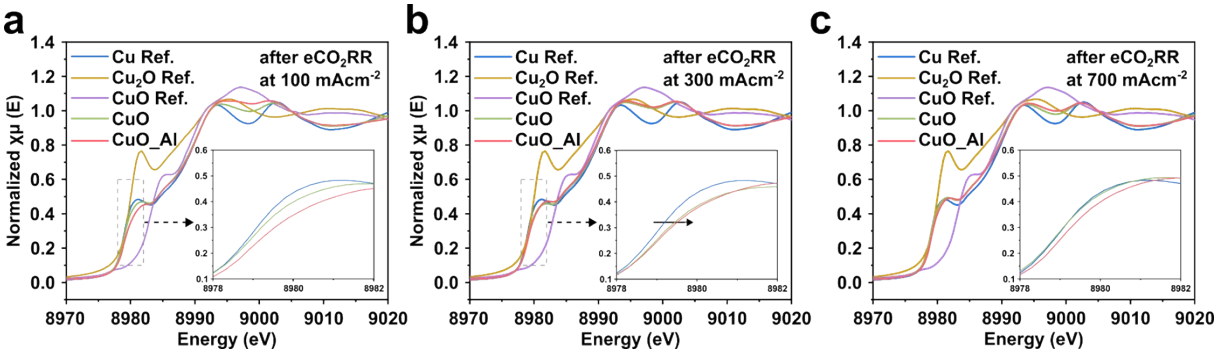

Figure S17. Cu K-edge XANES spectra of both catalysts at (a) 100 mA cm^{-2}, (b) 300 mA cm^{-2}, and (c) 700 mA cm^{-2}. The insets magnify the absorption edge of both catalysts at each current density.

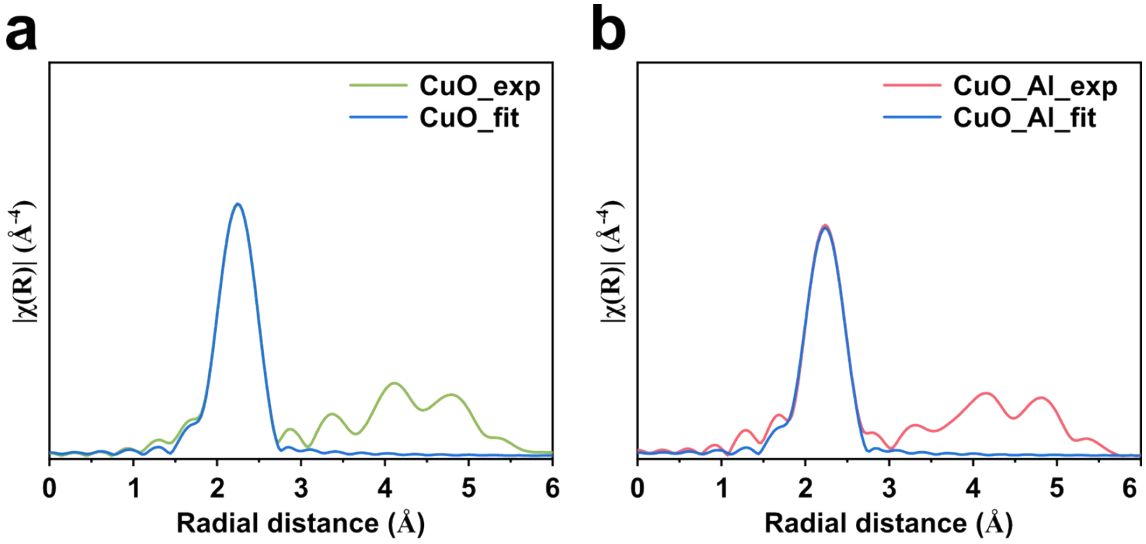

c

Element	Shell	CN	R (Å)	σ^2 (10^{-3} Å^2)
CuO	Cu-Cu	7.68 ± 0.22	2.54 ± 0.002	8.5 ± 0.2
CuO_Al	Cu-Cu	6.76 ± 0.33	2.54 ± 0.006	8.5 ± 0.7

Figure S18. Fitting curves for the Cu K-edge FT-EXAFS spectra of (a) CuO and (b) CuO_Al after eCO_2RR at 500 mA cm^{-2}, and (c) fitting parameters of both catalysts.

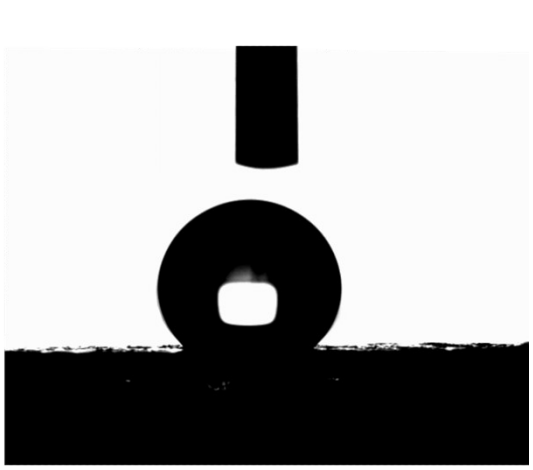

c

Electrocatalyst	Contact angle (°)
CuO	129.7
CuO_Al	131.5

d

Electrocatalyst	Contact angle (°)
CuO	112.8
CuO_Al	128.5

Figure S19. Photographs of the droplet on (a) CuO and (b) CuO_Al electrode before eCO_2RR for the contact angle determination and measured contact angles of CuO and CuO_Al (c) before and (d) after eCO_2RR.

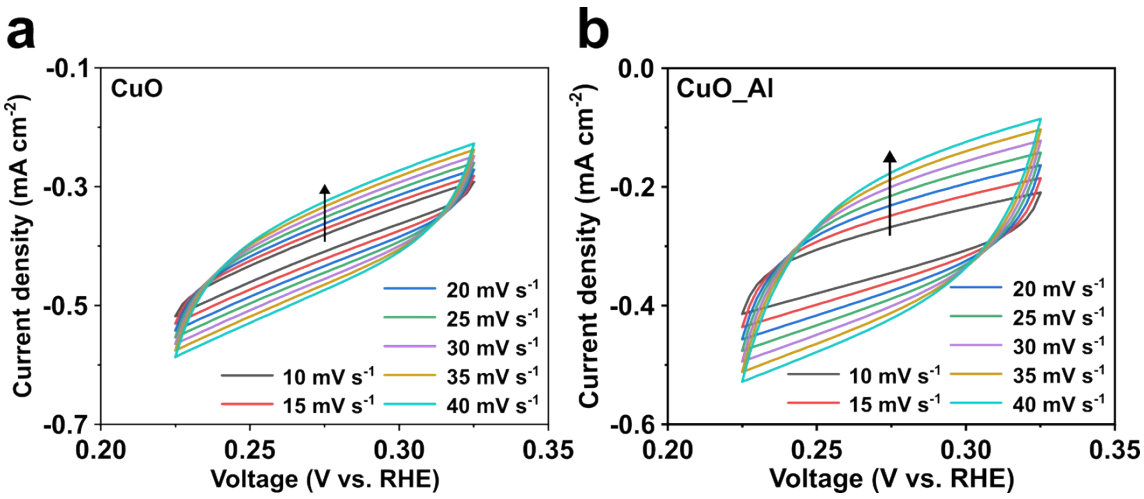

Figure S20. CV curves of (a) CuO and (b) CuO_Al after eCO_2RR for the determination of double-layer capacitance.

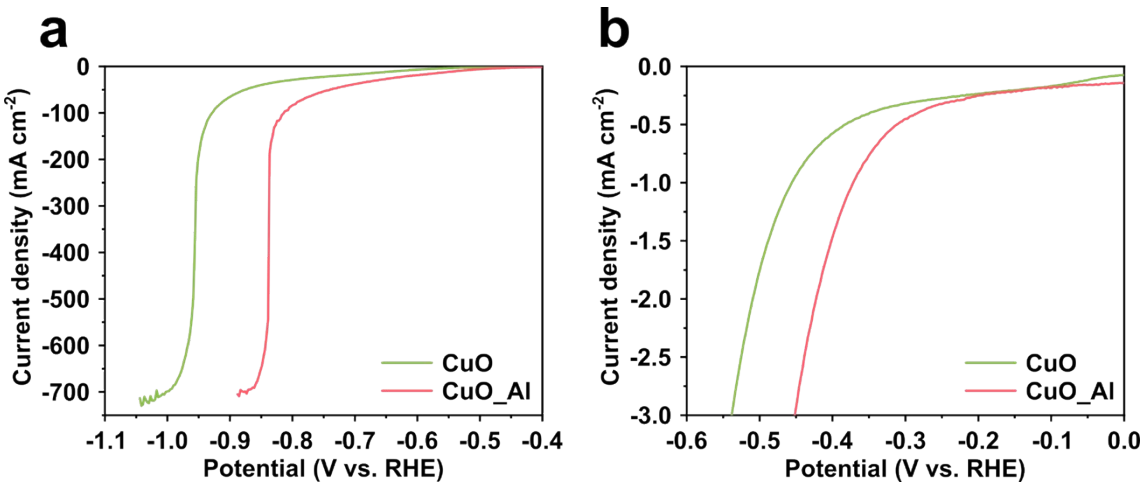

Figure S21. LSV curves of both catalysts in the potential range of (a) -0.4 V to -1.1 V (mass transfer limited potential) and (b) 0 V to -0.6 V indicating onset potentials.

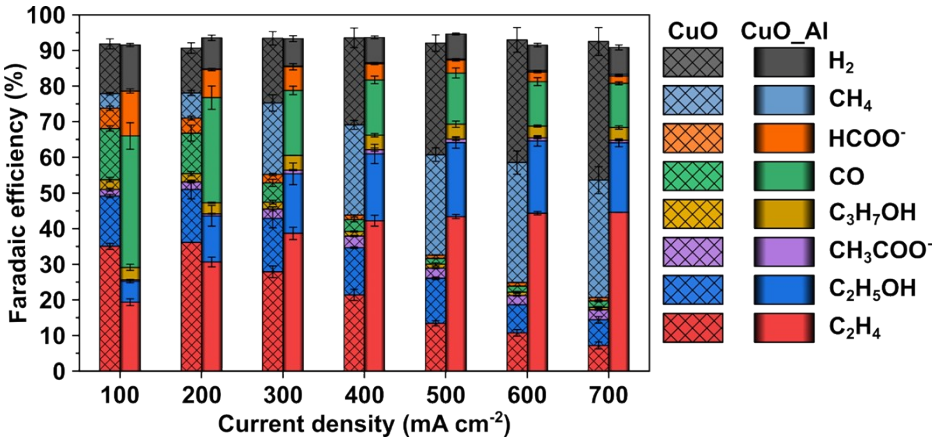

Figure S22. Faradaic efficiencies for various products as a function of geometric current density by both catalysts in 1M $KHCO_3$. The error bars correspond to the standard deviations calculated from three independent measurements.

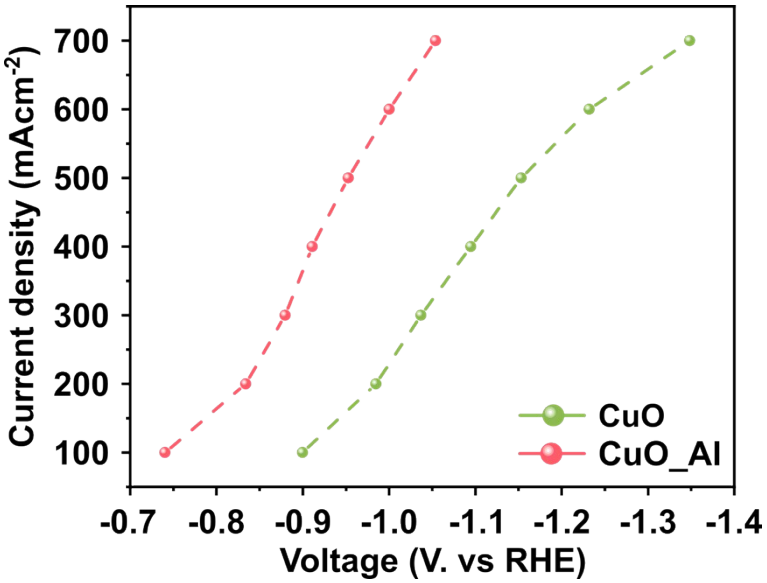

Figure S23. The current densities of both catalysts with 100 mA cm^{-2} step as a function of potential versus the reversible hydrogen electrode for comparing overpotentials.

a

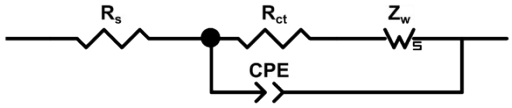

b

Electrocatalyst	R_s (Ω cm^2)	R_{ct} (Ω cm^2)
CuO	9.843	19.61
CuO_Al	9.473	5.67

Figure S24. (a) Equivalent circuit for fitting the Nyquist plots in Figure 2d and (b) calculated resistances by the fitting.

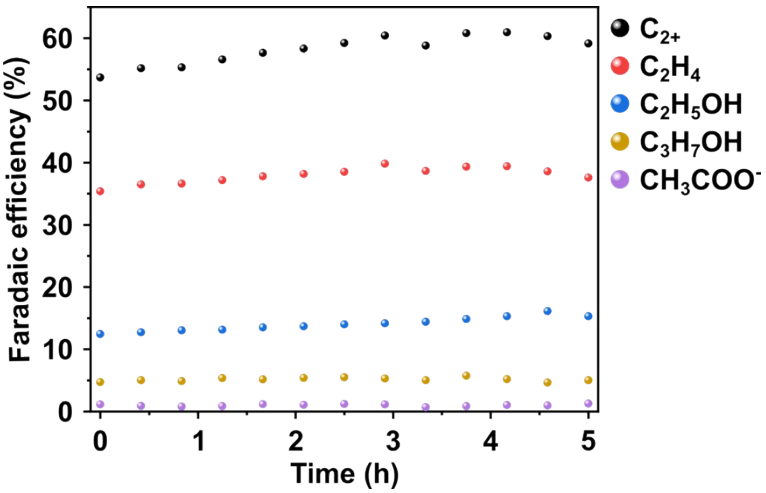

Figure S25. Faradaic efficiencies of C_2 products in CuO_Al long-term electrolysis at the current density of 300 mA cm^{-2} for 5 h.

To measure the Faradic efficiencies of C_2 liquid products, electrolytes were sampled in the middle of measurement.

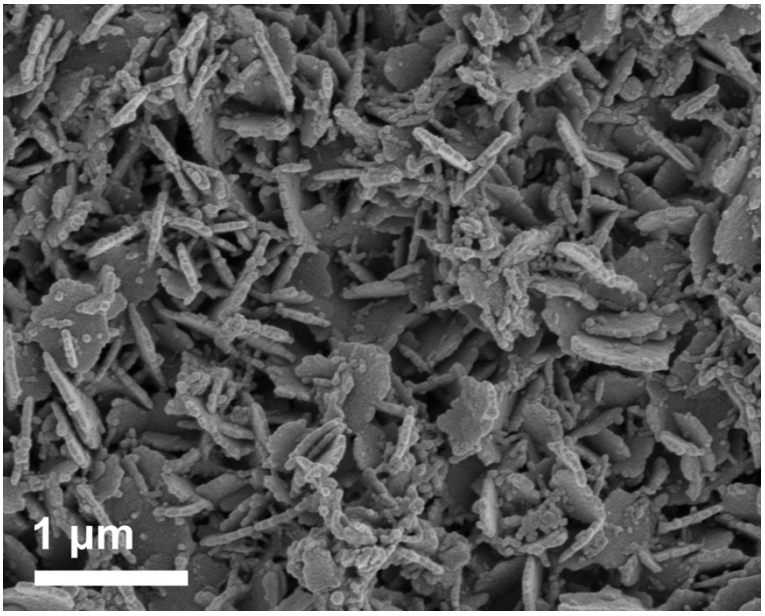

Figure S26. SEM image of CuO_Al after eCO_2RR for 5 h.

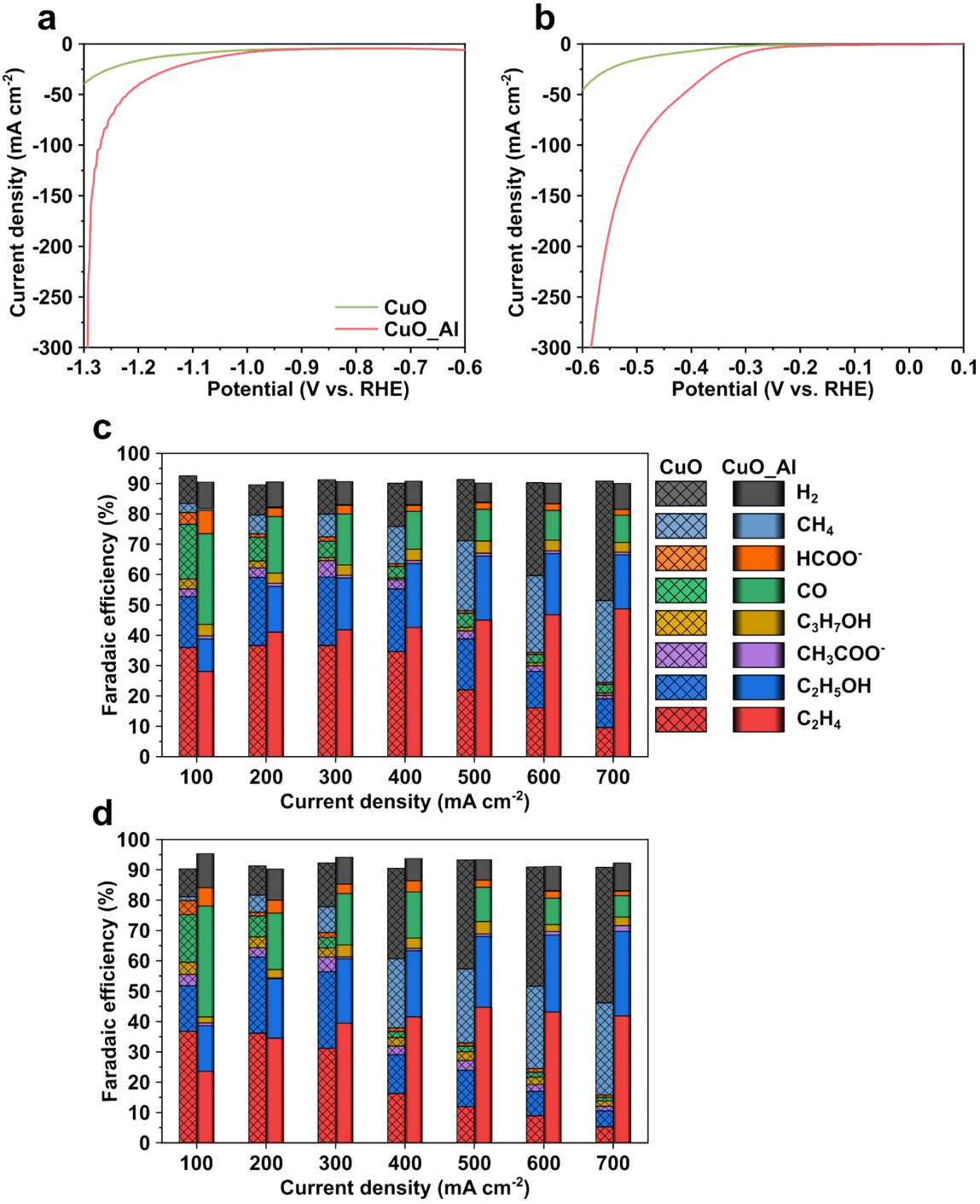

Figure S27. Electrocatalytic performance of CuO and CuO_Al in 0.5 M K_2SO_4 (pH adjusted to 2.0 with sulfuric acid) and 1 M KOH electrolytes using a flow cell electrolyzer. LSV curves at a scan rate of 10 mV s^{-1} in (a) 0.5 M K_2SO_4 and (b) 1 M KOH electrolytes. Faradaic efficiencies of various products as a function of geometric current density in (c) 0.5 M K_2SO_4

and (d) 1 M KOH electrolytes.

FE tendencies of both catalysts in 0.5 M K_2SO_4 and 1 M KOH are similar to FE tendencies of both catalysts in 1 M $KHCO_3$. C_{2+} FE of CuO_Al increased gradually with current density until 500 mA cm^{-2} and C_{2+} FE of CuO diminished steadily after 200 mA cm^{-2}. Also, H_2 and C_1 products FEs of CuO_Al decrease steadily with current density until 500 mA cm^{-2} and H_2 and C_1 products FEs of CuO rise steadily with current density from 200 mA cm^{-2}. Remarkably, CuO_Al showed superior performance in acidic 0.5 M K_2SO_4. Although bulk electrolyte is acidic, high eCO_2RR current density induces a mildly alkaline local environment near the cathode, which prevents catalyst dissolution in acidic electrolyte and suppresses hydrogen evolution reaction.[8]

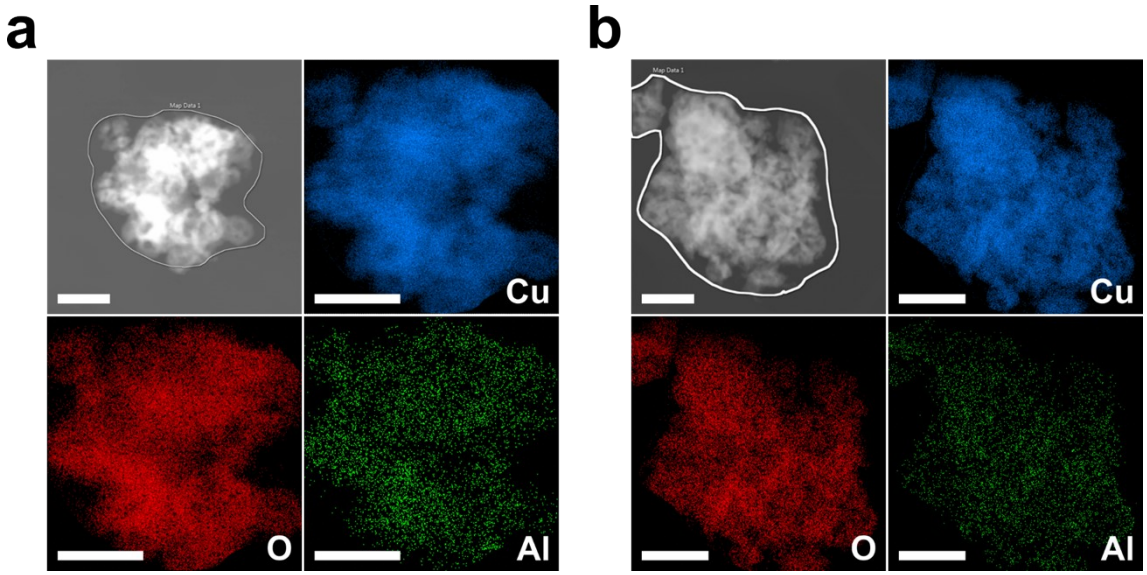

Figure S28. TEM images and corresponding EDS mapping images of CuO_Al with $Al(acac)_3$ precursor amounts of (a) 0.25 mmol and (b) 0.45 mmol.

Element	$Al(acac)_3$ 0.25 mmol (wt%)	$Al(acac)_3$ 0.35 mmol (wt%)	$Al(acac)_3$ 0.45 mmol (wt%)
Cu	99.34	99.19	99.04
Al	0.66	0.81	0.96

Table S3. Chemical compositions of Cu and Al in CuO_Al with different $Al(acac)_3$ precursor amounts by ICP-AES.

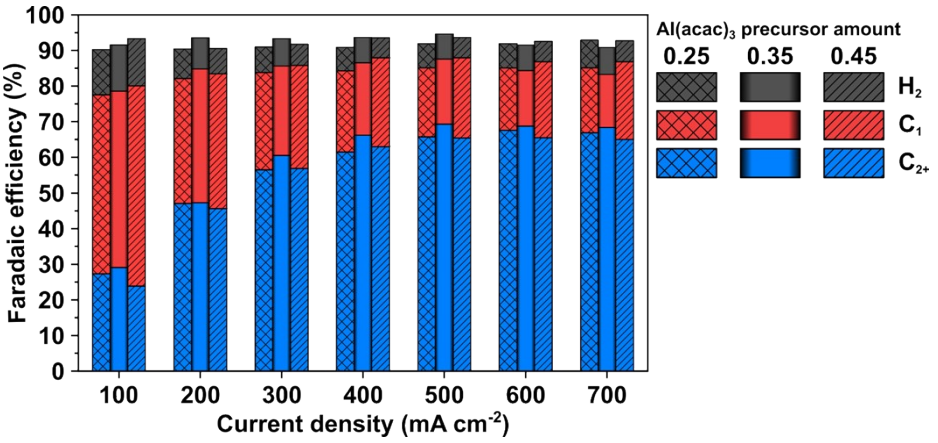

Figure S29. Faradaic efficiencies for H_2, C_1, and C_{2+} products at various current densities by CuO_Al with different $Al(acac)_3$ precursor amounts.

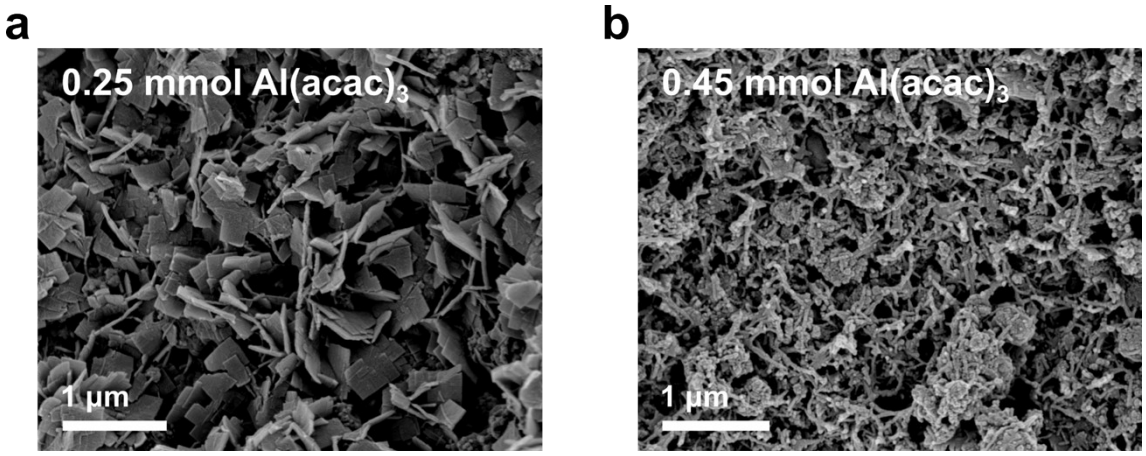

Figure S30. SEM images of CuO_Al with $Al(acac)_3$ precursor amount of (a) 0.25 mmol (b) 0.45 mmol.

References

1. D. H. Nam, O. S. Bushuyev, J. Li, P. De Luna, A. Seifitokaldani, C. T. Dinh, F. P. Garcia de Arquer, Y. Wang, Z. Liang, A. H. Proppe, C. S. Tan, P. Todorovic, O. Shekhah, C. M. Gabardo, J. W. Jo, J. Choi, M. J. Choi, S. W. Baek, J. Kim, D. Sinton, S. O. Kelley, M. Eddaoudi and E. H. Sargent, *J. Am. Chem. Soc.*, 2018, **140**, 11378-11386.
2. Y. Qiu, J. Zhang, J. Jin, J. Sun, H. Tang, Q. Chen, Z. Zhang, W. Sun, G. Meng, Q. Xu, Y. Zhu, A. Han, L. Gu, D. Wang and Y. Li, *Nat. Commun.*, 2021, **12**, 5273.
3. J. Choi, J. Kim, P. Wagner, S. Gambhir, R. Jalili, S. Byun, S. Sayyar, Y. M. Lee, D. R. MacFarlane, G. G. Wallace and D. L. Officer, *Energy Environ. Sci.*, 2019, **12**, 747-755.
4. C. Zhao, G. Luo, X. Liu, W. Zhang, Z. Li, Q. Xu, Q. Zhang, H. Wang, D. Li, F. Zhou, Y. Qu, X. Han, Z. Zhu, G. Wu, J. Wang, J. Zhu, T. Yao, Y. Li, H. J. M. Bouwmeester and Y. Wu, *Adv. Mater.*, 2020, **32**, e2002382.
5. Y. Li, D. Kim, S. Louisia, C. Xie, Q. Kong, S. Yu, T. Lin, S. Aloni, S. C. Fakra and P. Yang, *Proc. Natl. Acad. Sci. U. S. A.*, 2020, **117**, 9194-9201.
6. P. Sebastián-Pascual and M. Escudero-Escribano, *J. Electroanal. Chem.*, 2021, **896**.
7. D. Wakerley, S. Lamaison, F. Ozanam, N. Menguy, D. Mercier, P. Marcus, M. Fontecave and V. Mougel, *Nat. Mater.*, 2019, **18**, 1222-1227.
8. Y. Xie, P. Ou, X. Wang, Z. Xu, Y. C. Li, Z. Wang, J. E. Huang, J. Wicks, C. McCallum and N. Wang, *Nat. Catal.*, 2022, **5**, 564-570.